Permutation entropy and statistical complexity analysis of turbulence in laboratory plasmas and the solar wind

P. J. Weck, D. A. Schaffner, M. R. Brown, and R. T. Wicks

Permutation Entropy and Statistical Complexity Analysis of Turbulence in Laboratory Plasmas and the Solar Wind

P.J. Weck, D.A. Schaffner, and M.R. Brown

Swarthmore College, Swarthmore, PA 19081

R.T. Wicks

NASA Goddard Space Flight Center, Greenbelt, MD 20771

The Bandt-Pompe permutation entropy and the Jensen-Shannon statistical complexity are used to analyze fluctuating time series of three different turbulent plasmas: the magnetohydrodynamic (MHD) turbulence in the plasma wind tunnel of the Swarthmore Spheromak Experiment (SSX), drift-wave turbulence of ion saturation current fluctuations in the edge of the Large Plasma Device (LAPD) and fully-developed turbulent magnetic fluctuations of the solar wind taken from the *Wind* spacecraft. The entropy and complexity values are presented as coordinates on the CH plane for comparison among the different plasma environments and other fluctuation models. The solar wind is found to have the highest permutation entropy and lowest statistical complexity of the three data sets analyzed. Both laboratory data sets have larger values of statistical complexity, suggesting these systems have fewer degrees of freedom in their fluctuations, with SSX magnetic fluctuations having slightly less complexity than the LAPD edge I_{sat}. The CH plane coordinates are compared to the shape and distribution of a spectral decomposition of the waveforms. These results suggest that fully developed turbulence (solar wind) occupies the lower-right region of the CH plane, and that other plasma systems considered to be turbulent have less permutation entropy and more statistical complexity. This paper presents the first use of this statistical analysis tool on solar wind plasma, as well as on an MHD turbulent experimental plasma.

I. Introduction

Since Bandt and Pompe introduced their probability distribution based on ordinal patterns in arbitrary time series in 2002 [1], their methodology has found a wide variety of applications, from tracking the effects of anesthetic drugs on the brain [2–4] to informing economic policy [5–7] to various other areas [8–12]. In 2007, Rosso *et al* used the ordinal pattern distribution of Bandt and Pompe to construct the complexity-entropy plane, or "CH plane" whose horizontal coordinates are the computed values of the permutation entropy and whose vertical coordinates are the statistical complexity. This plane provides a graphical framework on which to compare time series from periodic, chaotic, and stochastic systems [13]. The CH plane has been used to determine the statistical character of fluctuations in several plasma systems, including magnetic flux ropes [14] and electron heat transport [15]. However this approach has yet to be extended to the study of dynamical MHD turbulence, either in the solar wind or in laboratory MHD plasma. The purpose of this paper is to provide the CH plane coordinates for these turbulent systems and compare to previous results, as well as to further the interpretation of this analysis tool for the study of turbulent plasma systems.

We compute the values of the permutation entropy and Jenson-Shannon statistical complexity for time series from three different turbulent plasmas, each with potentially different dominant physical mechanisms. First, we examine magnetic fluctuations in a spheromak of hydrogen plasma in the wind-tunnel configuration of the Swarthmore Spheromak Experiment (SSX). Then we analyze the density fluctuations on the edge of a helium plasma generated by a barium-oxide cathode source in the Large Plasma Device (LAPD). Finally, we compare both laboratory measurements to satellite measurements of the fluctuating magnetic field in the solar wind. The computed values of the permutation entropy and Jenson-Shannon complexity are then used as horizontal and vertical coordinates (respectively) on the CH plane, for comparison both across plasma systems and with well-known chaotic and stochastic models. The magnetic fluctuations in the solar wind are found to have the highest level of permutation entropy and lowest complexity, occupying a position on the lower right region of the CH plane nearest that of a purely random signal, which has zero complexity and maximal entropy. This result suggests that fully-developed turbulence, as the solar wind is thought to represent, can be identified by its proximity to maximal stochasticity on the CH plane. The LAPD edge fluctuations have the highest level of complexity of the three measured data sets and occupies a middle region in terms of the permutation entropy. Previous work has shown that the LAPD drift-wave turbulence may be dominated by non-linear interactions of relatively small numbers of modes, and thus tend to exhibit more chaotic, complex behavior [16]; thus, its coordinates occupy a position closest to known chaotic maps. Finally, the SSX fluctuations exhibit a level of complexity in between the other two plasmas. This suggests that the SSX plasma has more degrees of freedom in its fluctuations than the LAPD drift-wave plasma, but does not exhibit fully-developed turbulence, possibly because it is constrained by the laboratory boundaries. The permutation entropy of the SSX magnetic fluctuations is relatively high or low depending on whether fluctuations in dB/dt ($\dot{B}(t)$) or temporally

integrated B-field fluctuations (B(t)) are analyzed. This difference suggests that the level of entropy of a time series may be related to the rate of decrease in power as frequency increases.

It should be emphasized that, at this stage, the goal of this comparative study is to highlight the variations in outcomes using this particular analysis tool rather than attempting to unravel differences in the physical mechanisms underlying each dataset. In a sense, the work presented here was designed to be as physics-blind as possible. However, through study of how various mechanisms manifest in the complexity-entropy plane, a comprehensive physical understanding of each system can be pursued.

A description of how each dataset was generated is provided. The MHD wind tunnel configuration of the Swarthmore Spheromak Experiment (SSX) consists of a plasma gun which injects a spheromak of magnetized plasma into an ~ 1 meter long cylindrical copper flux conserver [17]. Probes embedded in the chamber collect data on turbulent fluctuations in $\dot{B}$ as the plasma evolves down the length of the tube, eventually relaxing into a Taylor state [17–20]. After injection the plasma is completely dynamical, as there is no guide or vacuum field in the body of the chamber. The $\dot{B}$ fluctuation signals for SSX were recorded by a 16-channel, 3-direction, single-loop pickup coil probe array embedded in the midplane of the cylindrical wind tunnel, with a 65 MHz sampling rate and 14 bit dynamic range. By varying the amount of magnetic flux through the core of the gun, referred to here as "stuffing flux", the magnetic helicity of the injected plasma can be finely controlled [19]. Magnetic helicity corresponds to the degree of twistedness in the magnetic field, so varying injected helicity affects the resulting turbulent dynamics of the plasma as it evolves towards a relaxed Taylor state.

While SSX primarily exhibits magnetic turbulence, many other plasma laboratories exhibit turbulent fluctuations of their density and temperature, typically generated by free energy in the gradients of these quantities. This form of turbulence is often referred to as pressure-gradient-driven, drift-wave or transport turbulence and is an important topic in fusion confinement studies [21]. Drift-wave turbulence can be studied in detail on the Large Plasma Device (LAPD) at UCLA [25]. LAPD generates a 17 m long, $\sim$60 cm diameter cylindrical plasma with a barium-oxide coated nickel cathode. In the data reported here, a plasma of density $\sim 2 \times 10^{12}$ cm^{-3} and peak temperature of 8 eV is produced in a uniform solenoidal magnetic field of 1000 G. Measurements of ion saturation current ($I_{\text{sat}} \propto n_e \sqrt{T_e}$) are taken with a 9-tip Langmuir probe (flush-mount tantalum tips) inserted radially into the edge of the cylindrical plasma produced by the source, a region where the turbulent fluctuations tend to be strongest. Signals were sampled at 1.5 MHz from a radial location of 26 cm [26]. The fluctuations in the edge are shown to be dominated by drift-wave modes due to the pressure gradient that develops between the plasma core and the chamber wall [27]. Since there is a strong background field in the LAPD, the magnetic fluctuations are not significant; thus fluctuations in the ion saturation current are used for this study.

Finally, we compare the laboratory plasma measurements of magnetic and drift-wave turbulence to observations from the *Wind* spacecraft of the turbulent solar wind. The *Wind* spacecraft provides high-cadence magnetic field observations of the solar wind using the MFI [22] from the L1 Lagrangian point between the Earth and the Sun. Measurements are made 11 times per second using a flux gate magnetometer and then averaged to 3 s to remove the spacecraft spin signal from the data. Flux gate measurements provide a DC magnetic field observation by measuring the bias required for no current to flow in a coil of wire subject to a changing magnetic field. Thus the observations are equivalent to B(t) observations made in SSX, rather than $\dot{B}$. The solar wind is highly variable but there are two broad types: fast wind (V > 600 km/s) which is emitted from open coronal field lines and is typically low density (< 5 protons/cm^3), has few large scale structures and has high amplitude but less developed turbulence, and slow wind, (V < 500km/s) which is typically found in the ecliptic plane and originates from more complex coronal magnetic topology and is denser and more structured than the fast wind with more evolved but lower amplitude turbulence [23, 24]. Here we use multi-day long intervals of a fast wind stream (Jan 14 - Jan 21 2008) and a slow wind stream (Jan 24 - Jan 29 2010) with large scale magnetic fluctuations on the order of 10 nT.

II. Permutation Entropy and the CH Plane

Bandt-Pompe permutation entropy and Jensen-Shannon statistical complexity are statistical metrics which measure two distinct properties of a dataset. Permutation entropy represents the randomness inherent in a process as displayed by discrete measurements of a parameter of the system. The greater the tendency of the system to repeat just a few fluctuation patterns in the measured signal (i.e. the more predictable it is), the lower its permutation entropy. Conversely, the more a system tends to exhibit all possible fluctuation patterns in the measurements (i.e. the more unpredictable it is), the higher the permutation entropy. On the other hand, for a given entropy, the Jensen-Shannon statistical complexity measures the degree to which there exist privileged fluctuations among those accessible to the system. By calculating both quantities for a given time series, valuable information can be gained simultaneously about the randomness of fluctuations in the system and the degree of correlational structure in these fluctuations.

The permutation entropy of an arbitrary time series is defined in terms of a window length called the embedding dimension n. The embedding dimension determines

the size of patterns investigated in calculating the entropy and complexity of the series. The instances of each ordinal patterns of that size are counted in order to associate an ordinal pattern probability distribution with the time series, from which the calculation of entropy and complexity is straightforward.

For embedding dimension n, the probability distribution introduced by Bandt and Pompe consists of the frequencies of occurrence of all possible length n ordinal patterns in segments of n consecutive terms from an arbitrary time series [1]. In their methodology, a length n ordinal pattern is defined for a segment $s = (x_t, x_{t+1}, \ldots, x_{t+(n-1)})$ of the time series as the permutation π of the index set $\{0, 1, \ldots, n-1\}$ corresponding to the ranking of the x_i in ascending order, namely $x_{\pi_t} < x_{\pi_{t+1}} < \ldots < x_{\pi_{t+(n-1)}}$. In order to guarantee a unique result, if $x_i = x_j$ where $i < j$, then in the ranking $x_i < x_j$. For example, if $x_0 = 5$, $x_1 = -2$, and $x_2 = 0.33$ are three consecutive terms in the time series, then since $x_1 < x_2 < x_0$, the ordinal pattern for this segment is the permutation $\pi = (1, 2, 0)$. Given a time series of length L, the corresponding ordinal pattern probability distribution $P = \{p(\pi)\}$ is defined in terms of all $L - n + 1$ length n segments s in the series and all $n!$ permutations π of order n by

$$p(\pi) = \frac{|\{s : s \text{ has ordinal pattern } \pi\}|}{L - n + 1}. \tag{1}$$

where $|\ldots|$ denotes the size of the set. The permutation entropy PE is defined as Shannon's information entropy for this ordinal pattern probability distribution, or

$$PE = -\sum^{n!} p(\pi) \log p(\pi) \tag{2}$$

where the log is base two.

Instead of considering consecutive points in calculating the ordinal pattern probability distribution for a time series, an embedding delay τ can be used to sample ordinal patterns on a larger time scale, thereby placing a lower limit on the temporal size of structures resolved, consequently limiting the maximum associated frequency. Embedding delays can be implemented as a simple subsampling of data in which only L/τ values of the time series are considered [14, 15] or all portions of the original time series can be used [28], a method referred to here as the length-preserving method. For example, for an embedding delay $\tau = 10$ using the former approach, a new time series X' of length $L' = \frac{1}{10}L$ is generated by selecting every tenth value of the original series X and the ordinal pattern probability distribution calculated for that series in the usual manner. In the length-preserving method, segments $(x_t, x_{t+10}, \ldots, x_{t+10(n-1)})$ of X are used to calculate the ordinal pattern probability distribution, where t runs from 1 to $L - 10(n-1)$, thereby including the 9/10ths of the dataset thrown out in the first method. Which method is used depends in part on the length of the record in question. Unless $L' \gg n!$, the

first method may not yield reliable statistics [14], and the length-preserving method thus appears preferable.

While the permutation entropy quantifies the randomness in an arbitrary time series, a measure of statistical complexity such as the Jensen-Shannon complexity is required to quantify any additional physical structure which might be reflected in the probability distribution constructed from the signal. The Jensen-Shannon complexity, or C_{JS}, of the distribution P of N probabilities associated with a time series is defined as the product

$$C_{JS}[P] = Q_J[P, P_e]H[P], \tag{3}$$

Where $H[P]$ is the normalized Shannon entropy and the quantity $Q_J[P, P_e]$ is a measure of disequilibrium, where $P_e = \{\frac{1}{N}, \ldots, \frac{1}{N}\}$ is the uniform distribution [29]. In other words, $Q_J[P, P_e]$ quantifies how different P is from an equiprobable distribution, characteristic of a system such as an isolated ideal gas [30]. Therefore the quantity $C_{JS}[P]$ will be nonzero only if there exist privileged states among those accessible to the system, and largest for a given entropy the further the distribution of accessible states is from uniform. Formally, once the disequilibrium is normalized such that $0 \leq C_{JS} \leq 1$, the Jensen-Shannon complexity can be expressed

$$C_{JS}[P] = -2 \frac{S\left[\frac{P+P_e}{2}\right] - \frac{1}{2}S[P] - \frac{1}{2}S[P_e]}{\frac{N+1}{N}\log(N+1) - 2\log(2N) + \log(N)} H[P], \tag{4}$$

Where S denotes the unnormalized Shannon entropy. When using the Bandt-Pompe methodology, the distribution P associated with the time series is the distribution of length n ordinal patterns, so that $N = n!$, $S[P] = PE$, and $H[P] = PE_{\text{norm}} = PE/\log n!$. C_{JS} can then be interpreted as a measure of the "non-triviality" of the frequencies of occurrence of ordinal patterns in the time series, reflecting underlying physical structures which would be excluded if only a measure of entropy were considered [29].

In order to develop some intuition about these metrics, it is often useful to consider simple examples. The simplest would be a monotonic time series, say representing a line with positive slope. The only length n ordinal pattern appearing in this time series is the permutation $(0,1,...,n)$, and thus the permutation entropy is $-1 \log 1 = 0$. The corresponding ordinal pattern probability distribution is far from a uniform distribution, with only one bin filled, so the disequilibrium is large. Nevertheless, C_{JS} is zero since PE is zero. The fact that a monotonic time series has zero complexity intuitively matches the characterization of the Jensen-Shannon complexity as a measure of structure, or non-triviality. At the other extreme is a completely random time series, from a maximally stochastic system where every possible ordinal pattern occurs with equal frequency $1/n!$. By construction, such a series maximizes the permutation entropy, so that $PE = \log(n!)$. However, the disequilibrium is

zero, so the C_{JS} also vanishes. This again intuitively fits with the identification of Jensen-Shannon complexity as a measure of correlational structure.

In intermediate systems with entropies between these extremes, there is a corresponding range of possible complexities. As shown in [13], by mapping out the positions of these systems on the CH plane $PE_{\mathrm{norm}} \times C_{JS}$, differing degrees of periodic, chaotic, and stochastic dynamics can be identified. As a functional of the entropy, C_{JS} is constrained between well-defined extremes for a given value of H [30, 31]. These crescent-shaped maximum and minimum complexity curves are shown in Figure 1. Within these bounds, regions of low entropy and low complexity are associated with predictable, orderly but unstructured dynamics, such as those of periodic systems. A time series generated from a sine function would occupy this region of the plane. Since a sine function must be discretized in order to generate a time series, ordinal patterns other than the basic monotonically increasing and decreasing patterns are introduced near the peaks and troughs. Therefore the permutation entropy and Jensen-Shannon complexity of a sine curve is nonzero, except in the limit of infinitesimal sampling. The middle to upper region of the plane, on the other hand is associated with relatively unpredictable systems which nevertheless possess a large degree of structure, manifested in a distribution of ordinal patterns which is far from uniform. This is the region of the CH plane occupied by deterministic chaos [13]. Finally, the lower-right region of the plane is associated with highly unpredictable systems which lack structure, in the sense that all possible ordinal patterns occur with more less the same frequency. Inherently probabilistic, or stochastic, models generally occupy this region of the plane. The less correlation between successive terms in a time series, the farther it tends towards the $PE_{\mathrm{norm}} = 1$, $C_{JS} = 0$ corner of the plane [13].

The $n = 5$ CH plane in Figure 1 includes the positions of several well-known models in order to illustrate each of these regions and provide some point of reference for subsequent comparisons of physical data. In particular, the CH positions of time series generated by a simple sine curve, chaotic Henon, skew tent, and logistic maps, and stochastic fractional Brownian motion (fBm) are shown. The three chaotic maps and fBm are described in Rosso 2007 [13]; the parameters used to generate time series in that publication are repeated here and are shown to occupy the same positions on the CH plane. Note that the dotted line corresponding to fBm was generated by varying the Hurst exponent, thereby scanning the degree of correlation between increments in the model from strong negative correlations to positive correlations.

III. CH comparison of SSX, *Wind*, and LAPD data

SSX magnetic fluctuations were analyzed over a 20 μs window during the stationary period of the discharge, corresponding to 1,300-sample records, and then aver-aged over 40 shots. Actual magnetic field fluctuations, B, are obtained by integrating the dB/dt signal over time. The normalized permutation entropy and Jensen-Shannon complexity were calculated for each series, using $n = 5$ in order to satisfy the common condition $L > 5n!$, as recommended in [32] and [33]. The length-preserving embedding delay method was employed to preserve this condition after sub-sampling. An embedding delay of $\tau = 8$ was used to filter frequencies above 9 MHz to avoid contamination from a high frequency noise mode inherent in the SSX plasma discharge, but small enough compared to the record length to avoid artificial numerical effects we found to be associated with small L/τ ratios. The average CH plane coordinate is computed from the individually computed coordinates of each orthogonal direction of the four innermost coil locations on the magnetic probe array. Two separate markers in Figure 1, one open and one filled, are shown in blue designating two different helicity settings. Error bars indicate standard deviations from the ensemble average.

Figure 1 also shows the positions of both fast and slow stream magnetic fluctuations in the solar wind. The fast stream magnetic signal from *Wind* consisted of almost $230,000$ values, and the slow stream signal of over $170,000$. Since both signals were highly stationary, a set of subseries could be treated as an ensemble. The length of subseries L_{wind} was chosen in conjunction with the embedding delay τ_{wind} so as to satisfy the condition $L_{wind}/\tau_{wind} = L_{ssx}/\tau_{ssx}$. Entropies and complexities were averaged over 20 subseries each $11,375$ values in length for the fast stream signal and 15 subseries of $11,375$ values for the slow stream. Delays of $\tau_{wind} = 70$ were used, which limits the upper frequency range of the dynamics under investigation to well within the inertial range. Error bars are within the range of the marker.

Previous work using frequency spectra has suggested that the edge fluctuations of magnetized plasmas in the LAPD and other devices are chaotic in nature [34]. The CH coordinate of the LAPD edge plasma shown in Figure 1 in red was averaged over 25 shots and 5 sections of 1000 values for each shot with no embedding delay.

The relative coordinates of each measurement show that the solar wind magnetic fluctuations at 1 AU are the most stochastic-like of the three with permutation entropy and complexity values of (H=0.964, C=0.057) for fast and (H=0.956, C=0.069) for slow wind, both close to that of pure white noise and more random than even classical Brownian motion, or fBm with Hurst exponent of 1/2 (fBm models have also been explored as a potential model for turbulent fluctuations in the solar wind and the magnetosphere [35]). The fast stream signal exhibits slightly more entropy and less complexity than the slow stream signal; it is as yet unclear whether this slight difference has a physical meaning, however. One possible hypothesis is that the higher incidence of uncorrelated Alfvenic fluctuations in the fast wind could contribute to a greater degree of stochasticity [36]. Al-
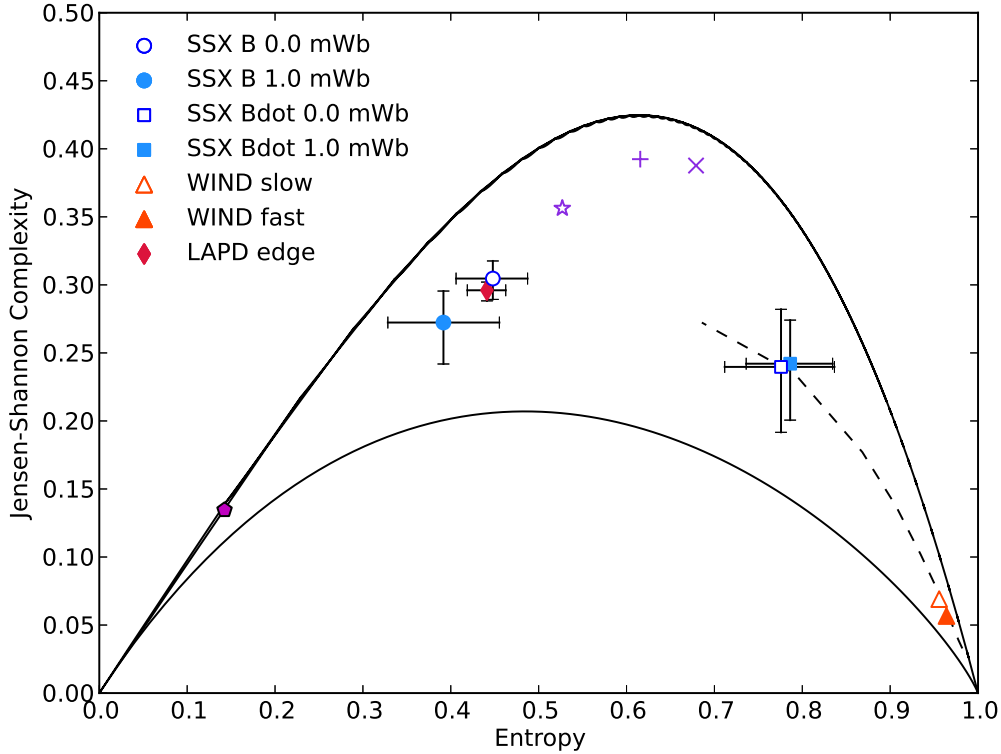
FIG. 1. (Color online) The $n = 5$ CH plane with SSX $\dot{B}$ and B (time-integrated from $\dot{B}$) data for two injected helicities, *Wind* fast and slow stream B data, LAPD edge plasma ion saturation current signals, and paradigmatic chaotic, periodic, and stochastic systems for comparison. The purple star, cross, and X markers represent chaotic skew tent, Henon, and logistic maps, respectively. The parameters used to generate time series for these chaotic maps are the same as in Rosso 2007 [13]. The pentagon marks the position of the Sine function, and stochastic fBm signals are indicated by a dashed black line. Crescent shaped curves show the maximum and minimum possible C_{JS} for a given PE_{norm}. Error bars indicate standard deviation from the ensemble average. Note that solar wind bars are smaller than the displayed size of the markers.

though it has been well documented that the solar wind exhibits well-developed turbulence [24], this is the first time that developed MHD turbulence in an astrophysical plasma has been identified based on the complexity-entropy plane analysis or compared in this manner to other plasma sources.

Conversely LAPD edge fluctuations are the most chaotic-like with coordinates of (H=0.441, C=0.296), closest of the three measurements to the chaotic models at the top of the CH plane. Although the complexity values for the full LAPD edge are slightly less than that observed in smaller drift-wave experimental setups [15], the relatively high complexity compared to the other measurements suggests a larger contribution from chaotic dynamics, likely associated with the non-linear interaction of the drift-wave modes [34].

Finally, SSX magnetic fluctuations have entropy/complexity values of (H=0.776, 0.786; C=0.24, 0.242) for $\dot{B}(t)$ data (0.0 and 1.0 mWb stuffing fluxes) and (H=0.448, 0.392; C=0.305, 0.272) for $B(t)$ (same

stuffing fluxes). The complexity values are in between that of LAPD and the solar wind, while the permutation entropy values differ substantially whether dB/dt or B is used. Naturally, this suggests that the magnetic fluctuations have a slightly more stochastic character than the density fluctuations of the LAPD edge, but do not reach the level of stochasticity of solar wind fluctuations. The large gap in entropy may be associated with the nature of the power spectrum, as will be discussed next.

The results of the CH plane analysis can be compared to a typical power spectrum analysis. Figure 2 shows the wavelet-generated power spectra [37] for the time series under investigation. Each spectrum is normalized to its minimum frequency in order for each curve to be placed on the same axis. This allows for the overall shape of the spectra to be directly compared. Furthermore, each curve is placed arbitrarily on the y-axis. Each spectrum is also cut-off at the frequency associated with the embedding delay used in the CH plane analysis. The LAPD
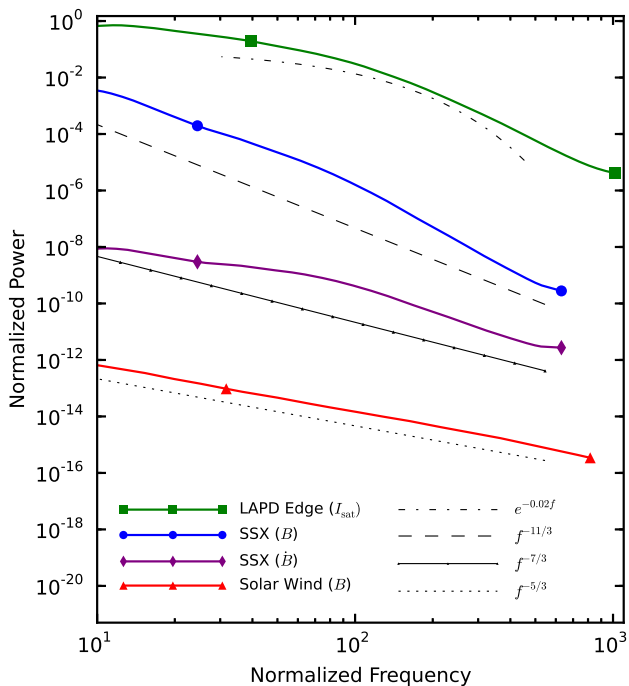
FIG. 2. (Color online) Spectra of LAPD edge I_{sat} fluctuations, SSX magnetic fluctuations and solar wind magnetic fluctuations are shown in thick lines with symbols. Each spectrum is normalized to a different time scale: LAPD is normalized to 500Hz; SSX is normalized to 12.8kHz; solar wind is normalized to 165μHz. Analytic forms for an exponential, a -11/3 power-law, and a -5/3 power-law (Kolmogorov) are indicated by the thin dashed lines. The power scale is arbitrary as the emphasis here is on the shape of the curves, not the relative power content of the spectra. The three spectra indicate a clear transition from exponential-like to power-law like broadband spectra. As an intermediate case, the SSX data exhibits both power-law behavior (steep and shallow) and exponential behavior (transition between steep and shallow).

spectrum shows the most exponential-like ($\sim e^{\tau f}$) shape while the solar wind spectrum is the most power-law like ($\sim f^{-\alpha}$). SSX $\dot{B}$ and B spectra are in between and would appear to have both power-law and exponential behavior. Previous work on SSX [20] has shown that the spectra has two power-law regimes, a steep and a shallow regime. The transition region, on the other hand, appears to have a somewhat exponential character to it. Since exponential spectra are typically identified with low-dimensional chaotic behavior [34], the range in spectra mirror the results of the complexity analysis. The most exponential spectrum (LAPD) has the highest level of complexity while the most power-law like (solar wind) has the least complexity and the SSX data, having potentially both power-law and exponential aspects, has complexities somewhere in between.

The spectra also shed light on interpretation of the permutation entropy. The steepest spectra in Fig 2 is the SSX B spectrum; the corresponding time series have the lowest entropies. The LAPD data, if it were compared to a power-law slope, would have the second steepest spectrum while the SSX $\dot{B}$ spectrum is third, and finally the solar wind is the shallowest. This ordering is consistent with the relative magnitudes of permutation entropy for each dataset. These results suggest that the permutation entropy is associated with the overall distribution of frequency power content of the time series, while the exponential versus power-law shape is associated with the level of complexity. It is clear that though each of these spectra is considered broadband and would perhaps be described as turbulent, the CH plane analysis reflects the different physical mechanisms which produce the fluctuations.

Next, the meaning of turbulence can be explored in the context of the CH positions of these fluctuations. The coordinates of solar wind magnetic fluctuations on the CH plane suggest that fully developed turbulence should occupy a region close to the stochastic limit. Meanwhile, while often referred to as turbulent, fluctuations in a laboratory setting (drift-wave turbulence for LAPD, MHD turbulence for SSX) may not be truly turbulent, or considered only weakly turbulent. Instead there appears to be a limit on how turbulent these fluctuations can be whether it is due to a limit on the number of modes associated with the fluctuations (as is thought to be the case in the LAPD [15]) or whether there is a limit on how much power can be distributed to higher frequencies (or smaller scales). In SSX, this latter issue may arise due to boundary or temporal development limits, both of which are not encountered by solar wind plasma (but may be relevant for the more bounded turbulent system of the magnetosheath [38, 39], for example). The results of the CH plane analysis highlight that more work is needed to push laboratory plasma turbulence research into the fully developed regime.

Finally, some discussion of how this analysis may be related to the typical measure of degrees of freedom in a turbulent plasma—Reynolds number—is warranted. Reynolds number, whether in reference to flow or magnetic turbulence (i.e. R_e or R_m), can be defined as the ratio of energy injection scale to energy dissipation scale in a turbulent cascade, and as such, can be interpreted as the number of degrees of freedom available to the system (or in other words, how many different scales energy can occupy between input and dissipation). The magnetic Reynolds number for the solar wind is typically on the order of 1×10^7 while SSX magnetic Reynolds numbers have been calculated (based on typical length scales and assuming Spizter resistivity as the dissipative mechanism) to be on the order of 1×10^2. Thus, Reynolds number shows a separation between solar wind data and SSX data though only in one dimension and qualitatively matches the difference in degrees of freedom suggested by the CH analysis. A complication arises when the LAPD data is introduced for comparison. Reynolds numbers are predicated on the separation of energy injection and dis-

sipation scales. However, drift-wave turbulence may not have a clear separation of scales as energy can potentially be injected or dissipated at different scales [40], and thus a Reynolds number may have less meaning in this case. The complexity-entropy analysis performed here, on the other hand, does not rely on any specific physical model and thus can be used to compare disparate systems.

IV.   Conclusion

In this paper, spectrally-broadband magnetic fluctuations in laboratory and astrophysical plasmas have been compared using the ordinal pattern-based CH plane introduced by Rosso *et al* for the first time. Comparing the relative coordinates of drift-wave, MHD wind tunnel, and solar wind plasmas, it was found that the three systems occupy different regions of the CH plane, suggesting that despite the broad-band spectra exhibited by all these systems, the CH analysis is capable of highlighting differences in the underlying nature of the fluctuations, particularly among drift-wave, partially developed, and fully developed turbulence. Drift-wave turbulence is thought to be a result of the nonlinear interactions of relatively few modes while fully developed turbulence contains too many modes to distinguish; it appears that the entropy-complexity analysis of these magnetized plasmas effectively highlights the number of degrees of freedom of the system in question. In particular, the smaller number of modes generating drift-wave turbulence in LAPD

edge plasmas are revealed by the low-middle entropy and middle-range complexity of that system, while the high entropy and low complexity of magnetic fluctuations in the solar wind may reflect the multitude of degrees of freedom active in that system. The analysis also showed that variations in permutation entropy may be related to power-law scaling of the spectra; in other words, permutation entropy may be proportional to the eveness of energy distribution among spectral frequencies. Based on the relative CH positions of SSX MHD wind tunnel and *Wind* data, although SSX is on its way towards the highly stochastic turbulence in the solar wind, this analysis indicates that further steps are needed for SSX to more accurately model solar wind turbulence. The confined nature of the experiment and short lifetimes involved are both potential contributors to the discrepancy in CH positions. Other than the boundary conditions imposed by astrophysical bodies, the solar wind is an unconfined and extremely long lived plasma. Whether one or both of these parameters could be varied to reduce the complexity and increase the entropy of SSX to that of the solar wind is an open question. In any case, the CH methodology has provided us with another avenue for comparing and understanding turbulence in plasmas.

[1] C. Bandt and B. Pompe. Phys. Rev. Lett. **88** 174102 (2002).
[2] D. Jordan, G. Stockmanns, E. F. Kochs, S. Pilge, and G. Schneider. Anesthesiology. **109** 1014 (2008).
[3] E. Olofsen, J.W. Sleigh, and A. Dahan. Br J Anaesth. **101** 810 (2008).
[4] D. Li, X. Li, Z. Liang et al. J Neural Eng. **7** 046010 (2010).
[5] A.F. Bariviera, L. Zunino, M. B. Guercio et al. J. Stat. Mech. Theor. Exp. **2013** P08007 (2013).
[6] L. Zunino, Z. Massiliano, B. M. Tabak et al. Physica A. **389** 1891 (2010).
[7] L. Zunino, B.M. Tabak, S. Francesco et al. Physica A. **390** 876 (2011).
[8] V. Suyal, A. Prasad, and H.P. Singh. Sol. Phys. 276 407 (2012).
[9] X. Sun, Y. Zou, V. Nikiforova et al. BMC Bioinformatics. **11** 607 (2010).
[10] P. M. Saco, L.C. Carpi, A. Figliola et al. Physicsa A. **389** 5022 (2010).
[11] M.C. Soriano, L. Zunino, O.A. Rosso et al. IEEE J. Quantum Electron. **47** 252 (2011).
[12] A.M. Kowalski, M.T. Martín, A. Plastino et al. Physica D. **233** 21 (2007).
[13] O.A. Rosso, H.A. Larrondo, M.T. Martin, A. Plastino, and M.A. Fuentes. Phys. Rev. Lett. **99** 154102 (2007).
[14] W. Gekelman, B. Van Compernolle, T. DeHaas, and S. Vincena. Plasma Physics. Cont. Fusion. **56** 064002 (2014).
[15] J.E. Maggs and G.J. Morales. Plasma Physics Cont. Fusion. **55** 085015 (2013).
[16] D.C. Pace, M. Shi, J.E. Maggs, G.J. Morales, and T.A. Carter. Phys. Plasmas. **15** 122304 (2008).
[17] T. Gray, M.R. Brown, and D. Dandurand. Phys. Rev. Lett. **110** 085002 (2013).
[18] D. A. Schaffner, V.S. Lukin, A. Wan and M.R. Brown. Plasma Physics Cont. Fusion. **56** 20 (2014).
[19] D.A. Schaffner, A. Wan, M.R. Brown. Phys. Rev. Lett. **112** 165001 (2014).
[20] D.A. Schaffner, V.S. Lukin and M.R. Brown. Astrophys. J. **790** 126 (2014).
[21] K. Burrell, Phys. Plasmas 4, 1499 (1997).
[22] R.P. Lepping, M.H. Acuna, L.F. Burlaga et al. Space Sci Rev. **71** 207 (1995).
[23] C.-Y. Tu, E. Marsch and H. Rosenbauer. Geophys. Res. Lett. **17** 283 (1990).
[24] R. Bruno and V. Carbone. Living Rev Solar Phys **10** (2013).
[25] W. Gekelman, H. Pfister, Z. Lucky, et al. Rev. Sci. Instrum. **62** 2875 (1991).
[26] D.A. Schaffner, T.A. Carter, G.D. Rossi et al. Phys. Rev. Lett. **109** 135002 (2012).
[27] J.E. Maggs and G.J. Morales GJ, Geophys. Res. Lett. **23** 633 (1996).
[28] C. Bandt. Ecol Model. **182** 229 (2005).
[29] Lamberti, P.W. and Martin, M.T. and Plastino, A. and

Rosso, O.A. Physica A **334** 119 (2004).

[30] R. López-Ruiz, H.L. Mancini, and X. Calbet. Phys. Lett. A. **209** 321 (1995).

[31] X. Calbet and R. López-Ruiz. Phys. Rev. E. **63** 066116 (2001).

[32] J. M. Amigó, S. Zambrano, M. A. F. Sanjuán. Europhys. Lett. **83** 60005 (2008).

[33] M. Riedl, A. Müller, and N. Wessel. Eur. Phys. J. Spec. Top. **222** 249 (2013).

[34] J.E. Maggs and G.J. Morales. Plasma Physics Cont. Fusion. **54** 124041 (2012).

[35] N.W. Watkins, D. Credgington, B. Hnat, S.C. Chapman, M.P. Freeman, J. Greenhough. Space Sci. Rev. **121** 271 (2005).

[36] S. Orlando, Y.Q. Lou, G. Peres, and R. Rosner. J. Geophys. Res. **102** 24139 (1997).

[37] C. Torrence and G.P. Compo. Bull. Am. Meterol. Soc. **79** 6178 (1998).

[38] F. Sahraoui, G. Belmont, L. Rezeau, et al. Phys. Rev. Lett. **96** 075002 (2006).

[39] E. Yordanova, A. Vaivads, M. Andre, S.C. Buchert, and Z. Voros. Phys. Rev. Lett. **100** 205003 (2008).

[40] B. Friedman, T.A. Carter, M.V. Umansky et al. Phys. Plasmas. **19** 102307 (2012).